

HAO LIANG, Rice University, USA

JOSUE ORTEGA CARO, Yale University, USA

VIKRAM MAHESHRI, Houston University, USA

ANKIT B. PATEL, Rice University, USA

GUHA BALAKRISHNAN, Rice University, USA

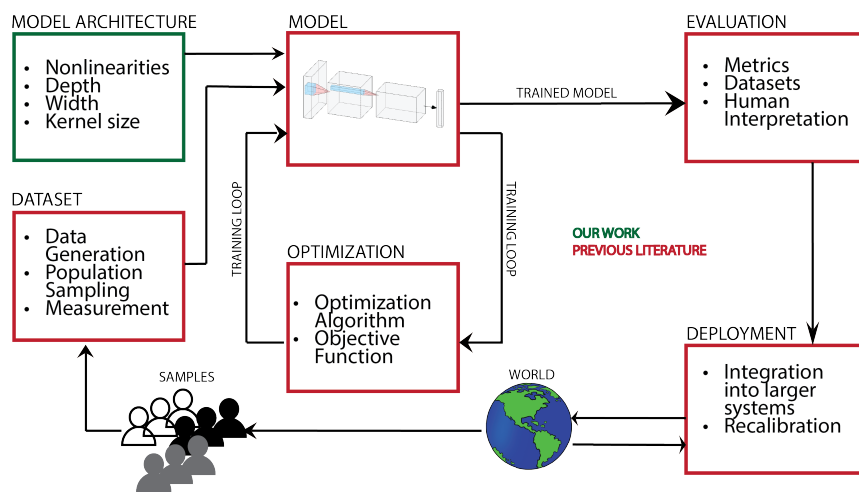


Fig. 1. **The deep learning model development pipeline.** Model development consists of many steps from data collection to evaluation and deployment. There has been a significant recent focus on understanding how datasets [1, 19, 47, 48, 71], evaluation procedures [26, 37], objective functions [34, 40, 45, 50, 64], and deployment decisions [44, 55] can influence a model’s fairness (red boxes). In contrast, there is virtually no research linking fundamental building blocks of deep learning model architectures (green box), such as their number of layers, convolutional kernel sizes, and activation functions, to algorithmic bias. In this paper, we establish a framework to measure causal effects of a model’s architectural hyperparameters on the biases learned by its features.

Training dataset biases are by far the most scrutinized factors when explaining algorithmic biases of neural networks. In contrast, hyperparameters related to the neural network architecture, e.g., the number of layers or choice of activation functions, have largely been ignored even though different network parameterizations are known to induce different *implicit biases* over learned features. For example, convolutional kernel size has been shown to bias CNNs towards different frequencies. In order to study the effect of these hyperparameters, we designed a causal framework for linking an architectural hyperparameter to algorithmic bias. Our framework is experimental, in that several versions of a network are trained with an intervention to a specific hyperparameter, and the resulting causal effect of this choice on performance bias is measured. We focused on the causal relationship between sensitivity to high-frequency image details and face analysis classification performance across different subpopulations (race/gender). In this

Permission to make digital or hard copies of all or part of this work for personal or classroom use is granted without fee provided that copies are not made or distributed for profit or commercial advantage and that copies bear this notice and the full citation on the first page. Copyrights for components of this work owned by others than ACM must be honored. Abstracting with credit is permitted. To copy otherwise, or republish, to post on servers or to redistribute to lists, requires prior specific permission and/or a fee. Request permissions from permissions@acm.org.

© 2023 Association for Computing Machinery.

Manuscript submitted to ACM

work, we show that modifying a CNN hyperparameter (convolutional kernel size), even in one layer of a CNN, will not only change a fundamental characteristic of the learned features (frequency content) but that this change can vary significantly across data subgroups (race/gender populations) leading to biased generalization performance even in the presence of a balanced dataset.

Additional Key Words and Phrases: high-frequency bias, model fairness, CNN

ACM Reference Format:

Hao Liang, Josue Ortega Caro, Vikram Maheshri, Ankit B. Patel, and Guha Balakrishnan. 2023. Towards causally linking architectural parametrizations to algorithmic bias in neural networks. In *Chicago '23: ACM Conference on Fairness, Accountability, and Transparency, June 12–15, 2023, Chicago, IL*. ACM, New York, NY, USA, 23 pages. <https://doi.org/XXXXXXX.12345>

1 INTRODUCTION

Algorithmic biases of a deep neural network, i.e., performance disparities across subgroups in the data distribution, are most often attributed to sampling biases in its training dataset where some groups of the data distribution have significantly lower or higher proportions than others. While an imbalance in the training data certainly has a strong influence on a deep network’s algorithmic bias [1, 11, 30, 48, 57, 71], it is just one factor in the development pipeline. Examples of other important factors in a model’s design include its parameterization and training objective function. While several previous works[3, 34, 40, 45, 50, 64] explore the impact of objective functions on bias and suggest fairness regularizers to include during training, a network’s parameterization, i.e., its particular functional form, has been virtually unexplored in the context of bias. A neural network has several parameterization hyperparameters that must be set by its designer, including the number of layers, activation functions, and convolutional kernel sizes in the case of a convolutional neural network (CNN). Each of these choices can affect the type of features learned by the model, which could in turn impact bias. In this work, we take a first step in showing how to causally link a neural network’s architectural hyperparameters to its algorithmic bias.

Different network parameterizations are known to induce different *implicit biases* over learned features. For example, several works demonstrate that CNNs tend to learn representations that are sensitive to high spatial frequency features of the input signal [8, 59, 66]. Based on the Fourier uncertainty principle, this phenomenon may be attributed to the size of the convolutional kernels [8] – smaller kernel sizes result in features that span a greater range in the Fourier domain. This implicit feature bias may be exposed by injecting a certain high-frequency signal into test images and observing a drop in the algorithm’s performance [63]. Implicit biases typically do not harm the model on within-distribution test samples because the parameters are well-tuned to the statistics in that distribution. The frequency noise/energy injection is essential to push the images *out-of-distribution* (OOD), thereby linking implicit biases to the *generalization performance* of the network. In this work, we show that in addition to this effect, implicit biases also affect the algorithmic bias of a network, such that features used by the network for one data subgroup may have significantly different characteristics for another. This in turn, can lead to disparate OOD performance on these groups.

The main contribution of our work is the design of a causal framework for linking an architectural hyperparameter of a neural network to its algorithmic bias. Our framework is based on an *experimental* procedure in which one or more parameters of a neural network architecture are modified at a time and the resulting bias on OOD samples are studied. First, we train from scratch multiple versions of the same neural network model that differ only in their choice of hyperparameter, e.g., convolutional kernel size. Second, we construct an OOD test set of images by injecting controlled perturbations to them, and obtain each model’s prediction on each image. The perturbation should be set based on the intended implicit feature bias being studied. For example, in our experiments, we use adversarial attacks and energy

injections in Fourier passbands to probe frequency implicit biases. Third, we fit a linear regressor to predict a model’s performance on an OOD test image as a function of the hyperparameter choice, degree of perturbation to the image, and various image attributes. Fourth and finally, we use the regression coefficients to measure the hyperparameter’s causal effects on model performances across data subgroups. This analysis provides a quantitative answer to whether the hyperparameter has a disparate causal effect on the data subgroups.

While our framework is general, we focused our experiments on studying the causal relationship between sensitivity to high-frequency image details induced by changes to convolutional kernel sizes and performance of face analysis classifiers across subpopulations (race/gender protected groups). We trained several research-grade face gender classifiers on public datasets, and show that modifying kernel size from a commonly used range: 3×3 to 11×11 even in just the first layer of these CNNs will not only change the frequency content of learned features, but that this change can vary significantly across race/gender groups. We established this effect using both adversarial perturbations and energy injections to the high-frequency bands of the test images. This work opens the door to further careful studies on understanding the impact of neural network design decisions on algorithmic bias.

2 RELATED WORK

2.1 Fairness in computer vision

There is a growing literature on fairness in computer vision. Studies predominantly focus on measuring and mitigating possible biases of computer vision models and datasets [1, 11, 19, 30, 47, 48, 57, 71]. Biases may be measured with a number of metrics [10, 21, 58] that quantify disparate performance differences of algorithms across population subgroups. Face recognition and analysis systems are often under the most scrutiny due to their sensitive nature [2, 29, 71]. Perhaps the most famous of these studies was “Gender Shades” study [6], which identified the systematic failings of face analysis systems on particular racial and gender demographics.

Image datasets are known to be biased due to sampling inequalities [1, 46, 57]. A dataset has sampling biases if its joint distribution of attributes is far from random. For example, the CelebA face dataset is known to have significant sampling biases, such as a higher proportion of female with young ages compared to male [2]. Training on such a dataset can cause a model trained on it to also have biases [29, 46, 67] particularly for attribute subgroups that are underrepresented in the dataset. Therefore, algorithmic fairness issues can be greatly mitigated if the algorithm is trained on a more balanced dataset. Human face datasets have been particularly scrutinized [2, 32, 35, 36, 43] as models trained on these data can exhibit systematic failings with respect to attributes protected by the law [33]. Multiple approaches to mitigate dataset bias include collecting more diverse examples [43], using image synthesis to compensate for distribution gaps [2, 36, 51, 54, 62, 71], and resampling [38]. Our work, in contrast, is focused on understanding biases of deep learning model decisions instead of data (see Fig. 1).

Researchers are also building novel computer vision model designs to combat biases [9, 16, 20, 23, 31, 38, 47, 49, 60, 61, 69, 72], typically by learning representations invariant to sensitive attributes via modified objective functions, or sampling in a balanced way during training. In contrast, our work is focused on linking how choices to fundamental building blocks of neural networks like kernel sizes and activation functions can affect algorithmic bias.

There are also lines of work outside of computer vision on mitigating biases of machine learning models. Outside of computer vision, the most common approaches add additional fairness measures to loss functions [3, 34, 40, 45, 50, 64], enforcing fair representations that are independent of protected attributes [4, 12, 41, 68], and augmenting training data

to promote balance [49]. None of these works try to establish a link between the functional components of a neural network to algorithmic bias.

2.2 Adversarial attacks

Neural networks have been shown to be surprisingly and stubbornly sensitive to imperceptibly small worst-case perturbations known as adversarial examples. An adversarial attack perturbs an image until a given network changes its prediction, usually by applying gradient descent on the image. The resulting changes to the image are high frequency, and imperceptible to the human eye (see Fig. 3). This lack of robustness has sparked many theories [5, 14, 15, 17, 18, 25, 42, 52, 56], but a unified theoretical explanation of the nature of adversarial examples is still lacking. Recent work has shown that commonly found adversarial examples for state-of-the-art convolutional neural networks contain dataset-specific information [59]. Furthermore, these adversarial attacks reflect properties of the features learned by the model [8], and that the model is biased towards certain features based on their architectural choice [13]. In this work, we analyze the information carried out by the attacks as a function of different architectural hyperparameter choices. Furthermore, we explore a novel hypothesis that adversarial attacks may allow us to expose differentiable information captured by a model’s features across different dataset subpopulations.

2.3 Frequency biases in CNNs

In image processing, the most common way to represent pixel location is in the spatial domain by column (x), row (y), and z (value). The frequency (or Fourier) domain offers an alternative perspective on the signal, by decomposing it in terms of sinusoids of varying frequencies. The Discrete Fourier Transform (DFT) is commonly used to transform an image between the spatial and frequency domain, and the inverse DFT may be used to transform in the opposite direction without loss of information.

Several recent works have provided new insights into the behavior of CNNs by studying the relationship between frequency content in input signals and a CNN’s predictions. For example, one finding is that high-frequency components play a significantly higher role in a CNN’s decision function and performance compared to human perception [59]. Another study showed that a contributing factor to this is that convolutional operations in CNNs will introduce an *implicit bias* towards using higher frequencies in an image [8]. Nonlinear activation functions such as the rectified linear unit (ReLU) could also be a contributing factor [27]. We build on the findings in these works to study the effect of frequency-based features in differentiable algorithmic performance across dataset subgroups like gender and race.

3 METHODS

Given a network architecture specification, and an architectural hyperparameter of interest, our goal is to uncover the causal effect of the hyperparameter on potential algorithmic biases due to an alteration of learned feature characteristics. We propose a framework to do this (see Fig. 2 for an overview). Our framework consists of three key steps. We first train K versions of the same network architecture that differ only by the choice of a single hyperparameter. The hyperparameter choice acts as a causal intervention, giving us an experimental rather than observational testing procedure. We then apply an out-of-distribution (OOD) perturbation to a set of test images that are annotated with various attributes of interest, including “protected” attributes (e.g., race and gender for faces) that we will use for bias analysis. Finally, we use a linear regression to predict some measure related to model predictions, given covariates such as the hyperparameter choice, image attributes, and OOD perturbation degree. We use the regression coefficients as estimates of causal effects of the various factors on the model, and specifically compare the differences between

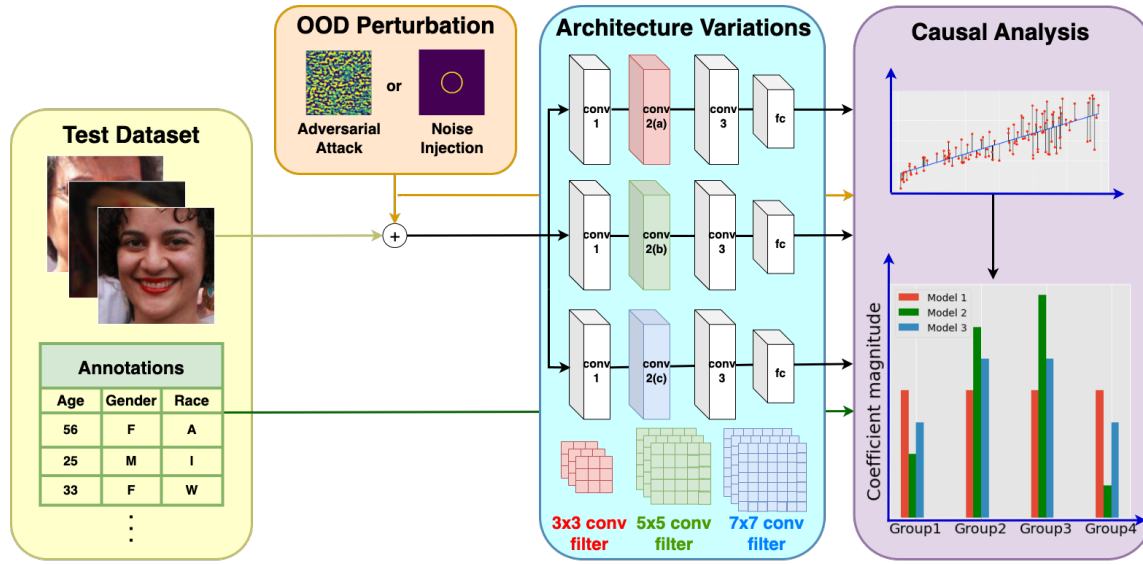


Fig. 2. **Method Framework.** The framework of our method consists of three parts. First, we perturb all the test images with Out Of Distribution(OOD) perturbations (in this work, we use adversarial attack perturbation and frequency noise injection), to make a new test dataset which contains the same images but with different noises injected. Second, we send the new test images to different models, where the models share most of the architecture design but differs only in some small part (e.g. convolutional kernel size). Last, we collect the results got from the last step and split them into according to sensitive attributes, and apply our causal analysis on the results.

coefficients corresponding to *protected* attributes to evaluate bias. We describe the three steps of our framework in the following sections.

3.1 Architecture training

We first train K different versions of the same architecture, all identical in structure except for a modification to the hyperparameter of interest. We train all architectures on the same training dataset. We also initialize the weights and biases of all networks from identical normal distributions (i.e., identical mean and variances). After the networks are trained, we “freeze” their parameters, and will not modify them further in our framework.

3.2 OOD perturbations to test data

Given various trained architectures, our goal is to amplify biases across their learned features. One option is to run test samples coming from the same distribution as the training data through these networks, and measure performance across different protected attribute subgroups. The problem with this strategy is that deep neural networks are over-parameterized, so that they are able to fit any training distribution nearly perfectly. Hence, even if a hyperparameter is altered from one network to another, both networks will likely yield similar performances on training data points.

However, as demonstrated in past works [63, 66], out-of-distribution (OOD) samples can paint a far different picture, with some models suffering in performance compared to others, thereby exposing differences across learned features. Therefore, a key step in our model is to inject a test set of images with a subtle class of perturbations so that they

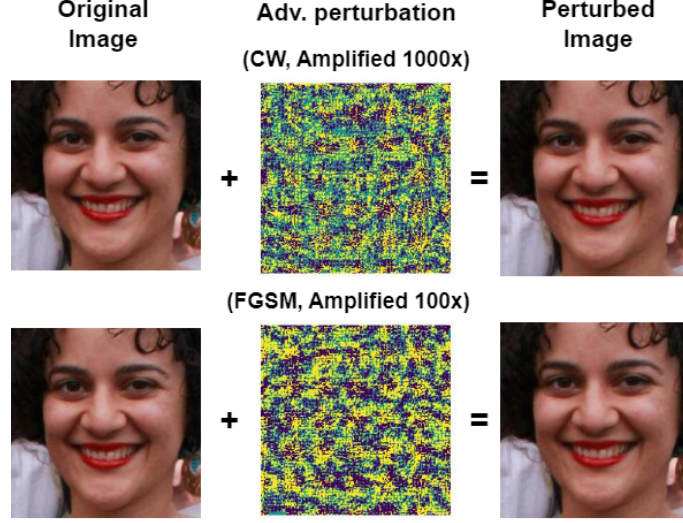


Fig. 3. **Example of adversarial attack perturbations.** By adding tiny noise-like perturbations (center image, amplified 100/1000 times for visualization) to a test image (left), a target neural network will output a wrong prediction. However, the perturbed image (right) has no perceptible differences with the original image to the human eye. We use the CW [7] and FGSM attacks [18] in our experiments.

become OOD. In our experiments, we focus on frequency-related implicit biases of CNNs, and so we consider two types of perturbations from the neural network literature: adversarial attacks, and frequency energy injections.

3.2.1 Adversarial attacks. We consider two types of adversarial attacks in our experiments. The first, **FGSM**[18], applies gradient descent on the loss of the network’s output with respect to the input image to “nudge” the image in incremental steps towards a direction that changes the network’s prediction. The second, **CW attack**[7], utilizes two separate losses: a gradient-based loss to make the classifier change its prediction (similar to FGSM), and a regularization to make the magnitude of the change to the image as small as possible. This makes the perturbation distance (i.e. l_2 norm of the difference between perturbed image and original image) of CW attack a useful metric for measuring the degree of difficulty to perturb an image. Fig 3 shows an example of a CW and FGSM attack for the same input image. Notice that the CW perturbation is an order of magnitude smaller due to the effect of its regularization.

3.2.2 Frequency energy injection. We also experiment with injecting energy to a specific frequency band to obtain a more fine-grained link between frequency content and network features. Fig. 4 depicts our process. For each test image, we use the DFT to obtain a Fourier spectrum, and amplify the amplitudes of Fourier coefficients lying on an annulus in the spectrum. In particular, let $F[\omega_x, \omega_y] = |A|e^{-j\phi}$ represent a complex coefficient in the Fourier spectrum of an image at location (ω_x, ω_y) (corresponding to x and y frequencies), with radius $r = \sqrt{\omega_x^2 + \omega_y^2}$, lying in the annulus defined by $(r - r_0)^2 \leq \Delta^2$. We increase the amplitude A by a factor of $1 + \delta$, to yield a modified coefficient $F'[\omega_x, \omega_y] = (1 + \delta)|A|e^{-j\phi}$. In our experiments, we set $\Delta = 2$, and $\delta = 15$ and $r_0 > 0$ is the frequency radius into which we are injecting energy. If r_0 is small (large), we are modifying low (high) frequency components of the image. Finally, we reconstruct the perturbed image using an inverse DFT.

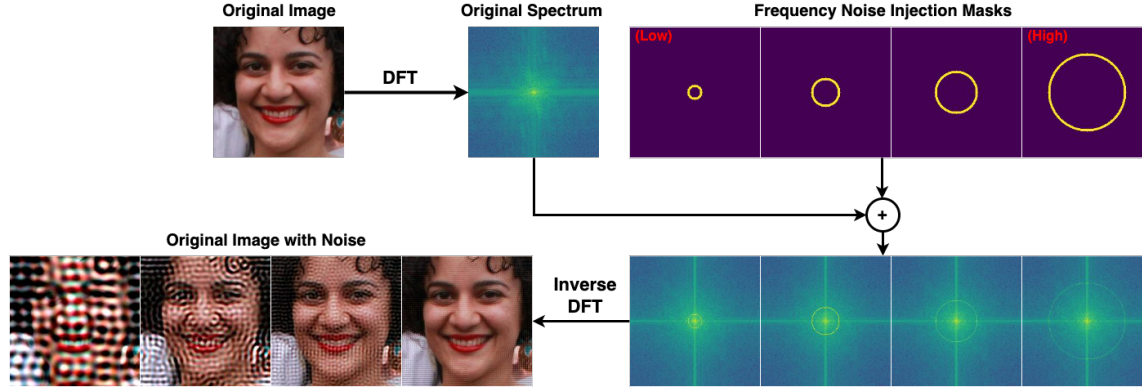


Fig. 4. **Examples of frequency energy injection perturbations.** Our goal with this perturbation is 'jitter' all frequencies with the same magnitude in an input image. To do this, we inject random noise to the Fourier coefficients of an image lying on an annulus of a particular radius in the Fourier spectrum (top row of annulus), according to: $(1 + \delta) |A| e^{-j\phi}$.

3.3 Causal analysis

We run the test set of OOD images through the K networks, yielding K predictions per image. We assume each image also comes with annotations for various relevant semantic attributes (including protected attributes with which we may compute algorithmic bias measures), as well as perturbation attributes (e.g., frequency of energy injection). Our goal is to measure the causal effects of the architectural hyperparameter of interest on model performance per protected attribute subgroup.

To do so, we use a multivariable linear regression model that predicts a dependent variable from multiple independent variables. For test image i processed in network k , let x_k be the corresponding hyperparameter and y_{ik} be a measure of network performance on image i . Then we can specify the following regression equation:

$$y_{ik} = \beta x_k + \epsilon_{ik}^0, \quad (1)$$

where ϵ_{ik} is an error term. Our coefficient of interest is β . Under the assumption that $E[x_k \cdot \epsilon_{ik}^0] = 0$, we can interpret β as the causal effect of network architecture on performance. Of course, this independence assumption is unlikely to hold, as image attributes, including the OOD perturbation value, will generally affect a neural network's performance.

We can weaken this assumption by leveraging a vector of image attributes Z_i , and augmenting equation (1) as follows:

$$y_{ik} = \beta x_k + Z_i' \gamma + \epsilon_{ik}^1, \quad (2)$$

where γ is a vector of coefficients, and β is now identified as the causal effect of network architecture on performance under the weaker assumption $E[x_k \cdot \epsilon_{ik}^1 | Z_i] = 0$. Moreover, we hypothesize that the effect of architecture hyperparameter x on performance may vary by protected attributes, a subset of all image attributes in Z_i . In order to allow for this possibility, we further augment equation (2) as follows:

$$y_{ik} = P_i' \beta x_k + Z_i' \gamma + \epsilon_{ik}^1, \quad (3)$$

where P_i is a vector of protected image attributes, and β is now a vector of coefficients. We use a heuristic approach to choose the vectors Z_i and P_i that is commonly used for causal inference in the social sciences [65]. First, we incrementally add controls to Z_i and test whether our estimates of β change under alternative specifications (using an F-test with the null-hypothesis that the estimates of β are equal across specifications). This is a test of the exogeneity assumption; if Z_i is a sufficiently rich vector of controls to satisfy $E[x_k \cdot \epsilon_{ik}^0 | Z_i] = 0$, then the assumption will also be satisfied conditional on an augmented vector of controls. Second, we start with a rich vector P_i to allow for the effect of network architecture on performance to be highly flexibly estimated. In our application, we begin by specifying P_i as a fully saturated vector of dummy variables corresponding to all protected attribute combinations (e.g., White Male, White Female, etc.) and estimate β . We then test whether the elements of β are equal to each other (using pairwise F-tests with null-hypotheses that pairs of elements of β are equal). To the extent that we are unable to reject equality of coefficients, we cannot reject that the effect of network architecture on performance varies across those two groups. For instance, if the coefficients on the “White Male” dummy variables and “Black Male” dummy variables are statistically indistinguishable from one another, then we cannot reject that the effect of network architecture on performance is the same for images of White males and images of Black males.

β encodes the joint causal effects of hyperparameter value x and protected attributes in P_i on output y . In particular, β_g is the expected change in y due to a unit change to x , when feature g is “True” (set to 1). In our experiments, we compare the values in β_g corresponding to different protected attribute subgroups to one another (see Table 2, and Fig. 9).

4 EXPERIMENTS & RESULTS

We evaluated our work on the task of gender classification from face images using two popular face analysis datasets: Fairface [28] and UTKFace [70]. Fairface was designed to contain a roughly equal number of samples from different race/gender groups, and has 86,744 training and 10,954 testing samples. FairFace contains labels for 7 race groups (‘East Asian’, ‘White’, ‘Latino Hispanic’, ‘Southeast Asian’, ‘Black’, ‘Indian’, ‘Middle Eastern’) and 2 gender groups (‘Male’ and ‘Female’). UTKFace contains 20,000 training and 3,705 testing samples, but is not balanced across race groups. It contains labels for 5 race groups (‘White’, ‘Black’, ‘Asian’, ‘Indian’, ‘Others’) and two gender groups (‘Male’ and ‘Female’). We remove faces from ‘Others’ because they have no consistent characteristics. To mitigate any effect of sampling biases during training, we used inverse sampling based on the number of examples from each race group. Training details are in Supplementary.

We demonstrate results using the ResNet-34 [22] base architecture for our experiments but obtained similar results using two other popular networks: DenseNet [24] and VGG-16 [53]. Please refer to Supplementary for results using these two models. Our architectural hyperparameter of interest was convolutional kernel size, a factor known to be related to implicit frequency biases of CNNs [8]. We considered two different scenarios: changing only the kernel size of the first layer and changing the kernel size of all layers simultaneously. Interestingly, both scenarios yielded similar results, and so we leave results for the latter in Supplementary. We varied the first layer kernel size (FLKS) within the range [3, 11], which encompasses the popular choices for this hyperparameter for nearly all CNNs in the literature. We initialize the weights and biases of all of our models randomly by drawing from a Normal distribution with variance set to 0.02. For each network and kernel size value, we trained 3 independent models and presented average results to mitigate the influence of random initialization factors.

We first report our networks’ accuracies for different race groups in Table 1 on *non-OOD* test images, to demonstrate that they all achieve reasonably high accuracies on both datasets. The performances do not significantly vary with

Table 1. **Model performances on *unperturbed* (non-OOD) images from the Fairface & UTKFace datasets.** We report the trained models’ performances on test sets split by race group. Each number is an average over 3 different trained models. The first column indicates the dataset name and model’s First Layer Kernel Size (FLKS). Fairface has 7 annotated race groups and UTKFace has 4. The performances are relatively constant with a variation to kernel size because the test and training images belong to the same distribution.

Dataset (FLKS)	Overall	White	Black	East Asian	Indian	Southeast Asian	Latino	Mid. Eastern
Fairface (3)	0.947	0.950	0.894	0.942	0.945	0.894	0.957	0.977
Fairface (5)	0.949	0.947	0.896	0.939	0.957	0.896	0.957	0.980
Fairface (7)	0.946	0.943	0.895	0.947	0.956	0.895	0.963	0.978
Fairface (9)	0.947	0.946	0.895	0.937	0.951	0.895	0.960	0.979
Fairface (11)	0.946	0.949	0.892	0.937	0.949	0.885	0.967	0.979
UTKFace (3)	0.929	0.949	0.905	0.931	0.942	/	/	/
UTKFace (5)	0.935	0.951	0.901	0.940	0.951	/	/	/
UTKFace (7)	0.934	0.955	0.905	0.939	0.953	/	/	/
UTKFace (9)	0.937	0.955	0.910	0.941	0.955	/	/	/
UTKFace (11)	0.936	0.950	0.901	0.943	0.955	/	/	/

FLKS because the training and testing images are all from the same distribution. We now present our results separately for the two OOD perturbations described in Sec. 3.2: adversarial attacks and frequency energy injections.

4.1 Adversarial attacks

We present results in this section using the CW adversarial attack. We obtained similar results using FGSM (see Supplementary).

4.1.1 Analyzing Fourier spectra. We first visualize the average Fourier spectra magnitudes of the adversarial perturbation images (e.g., center image in Fig. 3), split by race/gender groups and FLKS in Fig. 5 (for Fairface) and Fig. 6 (for UTKFace). Results on both datasets show similar trends. First, as FLKS increases, the spectral energy becomes more focused at low-frequencies (closer to center). Second, holding FLKS value constant, we see that the spectrum for the Black group consistently contains less high-frequency energy compared to the spectra of other race groups. This result also holds for the Male group compared to Female. The difference between different subgroups shrinks as FLKS increases, in line with findings from a previous study showing that low FLKS leads to higher implicit frequency bias [8].

To quantitatively assess differences in the perturbation spectra, we also compute the $f_{0.5}$ metric, known as “half power frequency,” or the frequency below which half of the signal’s power lies. $f_{0.5}$ is a robust measure of energy concentration in a spectrum. We show the $f_{0.5}$ scores for the spectra in Fig. 5 and Fig. 6 in Fig 7-top. The $f_{0.5}$ confirm the trend we observed visually. Please refer to the caption of Fig. 7 for more details.

4.1.2 Perturbation distances. We next present the average perturbation *distances* of adversarial attacks across race groups and models in Fig 7-bottom. The perturbation distance d_p between an original test image I and the perturbed image I' may be computed by simply taking an L2 norm: $d_p(I, I') = \|I' - I\|_2$, and quantifies how close/far the perturbed image to the original image. A larger distance indicates that more “work” must be done harder to fool the model, and its a reflection of the robustness of the model to other OOD perturbations [39].

Results show that perturbation distance increases with FLKS for all race groups, with an associated increase to variance. It is therefore harder to adversarially attack a model with a larger FLKS, likely because such a model focuses more of its energy on low-frequency image information (see Fig 5 and 6) and is therefore robust. In addition, we see

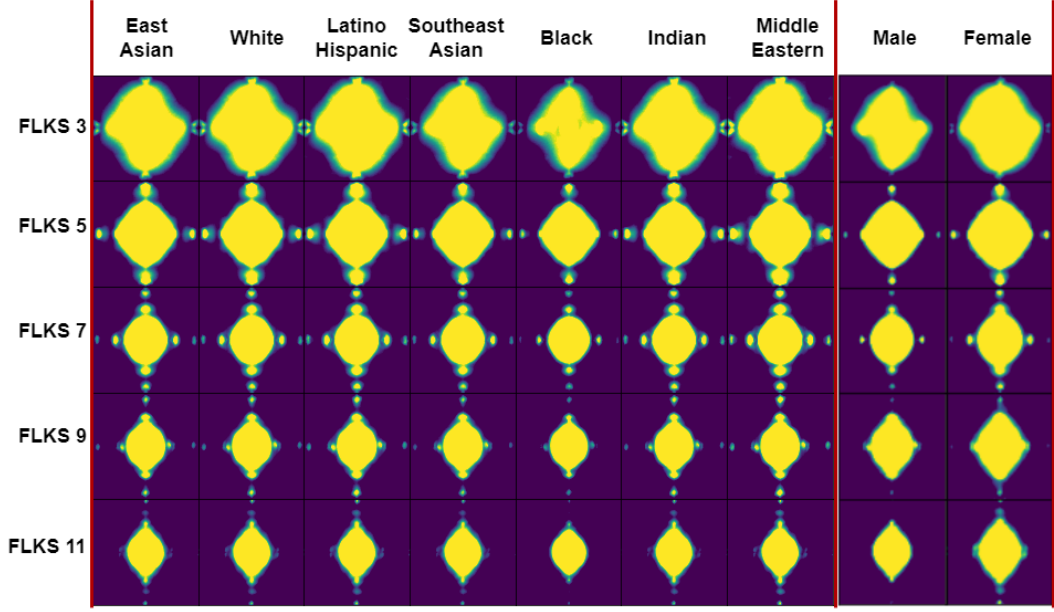


Fig. 5. **Average spectra of adversarial perturbation images split by race and gender for Fairface.** Each row represents a model with a different first layer kernel size (FLKS). As FLKS increases, the spectra become more concentrated at low frequencies. The spectra for the Black race group consistently have less energy at high frequencies compared to the spectra of other race groups. Male spectra also have lower high frequency information compared to Female spectra. These results demonstrate that changes to FLKS induce different feature biases for networks, which also vary by protected attribute subgroups. See Fig. 6 for the analogous spectra for the UTKFace dataset.

that d_p for the Black group is significantly lower than that of other groups. Please refer to the caption of Fig 7 for more details.

4.1.3 Causal analysis. Next, we quantitatively analyze the causal relationship between race and gender on perturbation distance d_p by applying our causal analysis framework introduced in Sec. 3.3. Specifically, using Eq. 3, we set y to be d_p , and set both P_1 and Z_1 to contain “dummy variables” corresponding to all race/gender combinations. We use the Fairface dataset for this analysis, and use the race groups East Asian, White, Latino Hispanic, Southeast Asian, Indian and Black, and gender groups of Male and Female. We ignore Middle Eastern since the numbers of samples for different genders are unbalanced in test dataset.

We use the *statsmodel* package from Python to run this regression, and we present the resulting values of β and γ in Table 2. The results of β are also shown in Fig. 9(a). Based on the results, it is obvious that the coefficients for Black and Indian are significantly higher than that of other race groups, indicating the impact of kernel size on perturbation distance is much more significant for the two groups. White, Black and Indian female have larger β values than their corresponding male group.

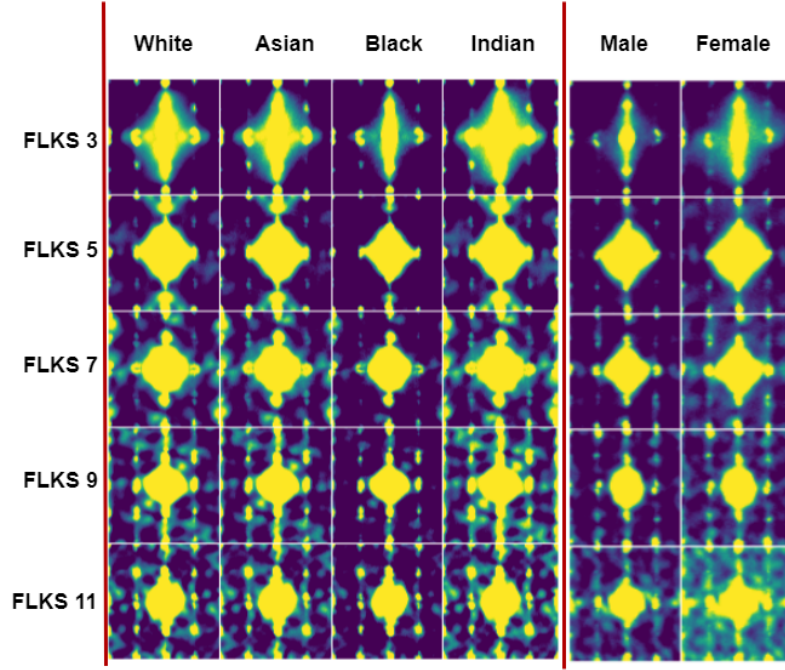


Fig. 6. **Average spectra of adversarial perturbation images split by race and gender for UTKFace.** We see similar trends in these spectra to the ones shown for Fairface in Fig 5.

Table 2. **Regression results of perturbation distance.** We report the coefficients β (left) and γ (right) for the regression described in Sec. 4.1.3. We also report the standard deviations of the coefficient values and calculate their t values according to $t = \frac{\text{coefvalue}}{\text{stderr}}$, as well as $P > |t|$. A $P \leq 0.05$ indicates the value is significant. The β coefficient names use subscripts corresponding to race (E: East Asian, W: White, B: Black, I: Indian, L: Latino, S: Southeast Asian), and gender (M: Male, F: Female). Some large disparities between β values across groups are obvious, e.g., the values for Black Asian Female is $\sim 100\%$ higher than that of East Asian Female. Refer to Fig. 9 for plots on β .

coef name	coef value	std err	t	$P > t $	coef name	coef value	std err	t	$P > t $
β_{EM}	0.0227	0.003	6.930	0.000	γ_{EM}	0.4251	0.025	17.308	0.000
β_{EF}	0.0274	0.003	8.323	0.000	γ_{EF}	0.4232	0.025	17.065	0.000
β_{WM}	0.0306	0.003	11.392	0.000	γ_{WM}	0.4453	0.020	21.969	0.000
β_{WF}	0.0254	0.003	8.614	0.000	γ_{WF}	0.4302	0.022	19.361	0.000
β_{LM}	0.0351	0.003	11.143	0.000	γ_{LM}	0.2088	0.012	17.566	0.000
β_{LF}	0.0269	0.003	8.521	0.000	γ_{LF}	0.2425	0.012	20.304	0.000
β_{SM}	0.0251	0.003	7.552	0.000	γ_{BM}	0.1856	0.013	14.783	0.000
β_{SF}	0.0189	0.004	5.982	0.000	γ_{BF}	0.2163	0.014	15.281	0.000
β_{BM}	0.0589	0.001	48.770	0.000	γ_{BM}	0.2088	0.012	17.505	0.000
β_{BF}	0.0659	0.001	48.588	0.000	γ_{BF}	0.2425	0.012	20.234	0.000
β_{IM}	0.0748	0.001	61.160	0.000	γ_{BM}	0.1856	0.013	14.783	0.000
β_{IF}	0.0846	0.001	65.294	0.000	γ_{BF}	0.2163	0.014	15.821	0.000

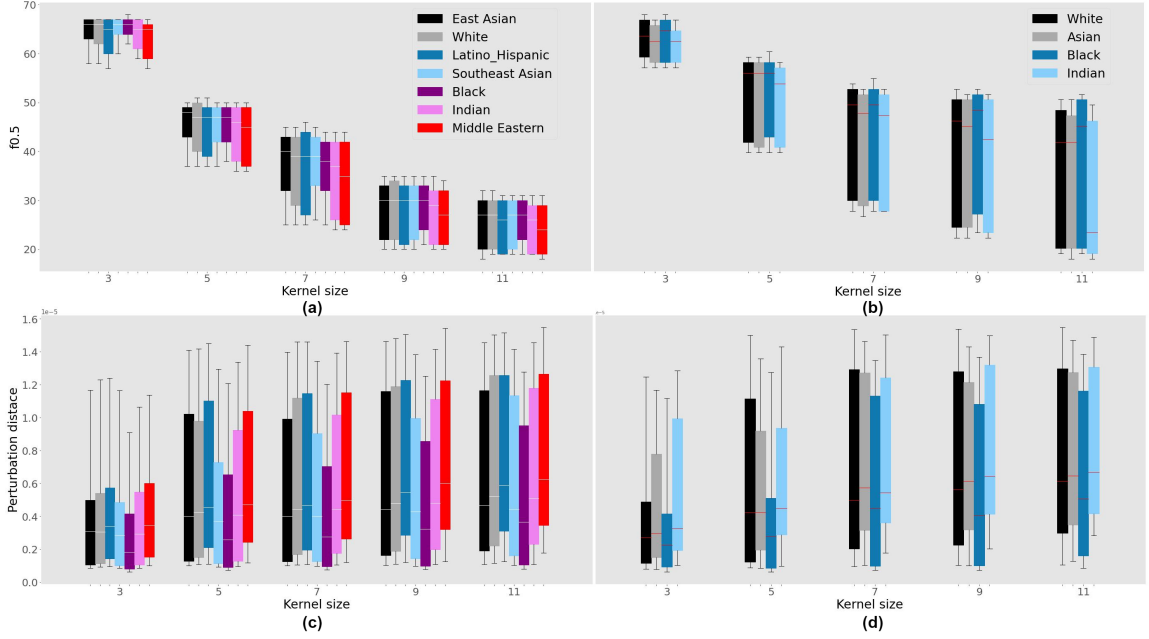


Fig. 7. $f_{0.5}$ measures for adversarial perturbation spectra & adversarial perturbation distance Each boxplot shows the median score (white/red line in the boxes) and the 15% – 85% confidence interval for a different protected attribute group. The x-axis for all plots indicates the models’ first layer convolutional kernel size (FLKS). (a) and (b) are $f_{0.5}$ measures for adversarial perturbations using Fairface and UTKFace, respectively. The $f_{0.5}$ score drops as FLKS increases for all demographic groups, which indicates that the adversarial attack focuses less on high-frequency information of the image for larger FLKS. (c) and (d) show the adversarial perturbation distances per race group using Fairface and UTKFace, respectively, where distance is simply the l_2 norm of the perturbation image. As the FLKS increases, the perturbation distances generally increase too for all the demographic groups. In addition, for each FLKS value, the perturbation distances for the Black group are always significantly lower than those for other demographic groups.

4.2 Frequency Energy Injection

We next perform the frequency-based OOD perturbation to the test images as described in 3.2.2 and visualize results in Fig 8. The results show that the accuracies of all models/groups are more influenced by perturbation for to low-to-mid frequencies ($0.02 - -0.20(Hz)$), and less so with mid-to-high frequencies. FLKS of 3 is less affected by frequency injections in the range ($0.08 - 0.15(Hz)$). In general though, it is difficult to ascertain significant trends from the plots alone.

4.2.1 Causal analysis. Similar to Sec. 4.1.3, we now perform a regression to measure the impact of kernel size, frequency of energy injection, and protected attribute subgroup on model error per image. Using Eq. 3, we set y to be the error rate of an image and set both P_i and Z_i to contain “dummy variables” corresponding to race/frequency (of injected energy) combinations. We use four frequency subgroups: $\{(0.05, 0.07), (0.09, 0.11), (0.13, 0.15), (0.17, 0.19)(Hz)\}$, which we label 1, 2, 3, 4 for convenience. We report the results of coefficient β values in Fig 9(b). It is clear that the coefficients for frequency group 4 are significantly smaller than those of the rest of the frequencies, indicating that changes to kernel size influence the performance less on the OOD samples under relatively high-frequency injections. The coefficient for

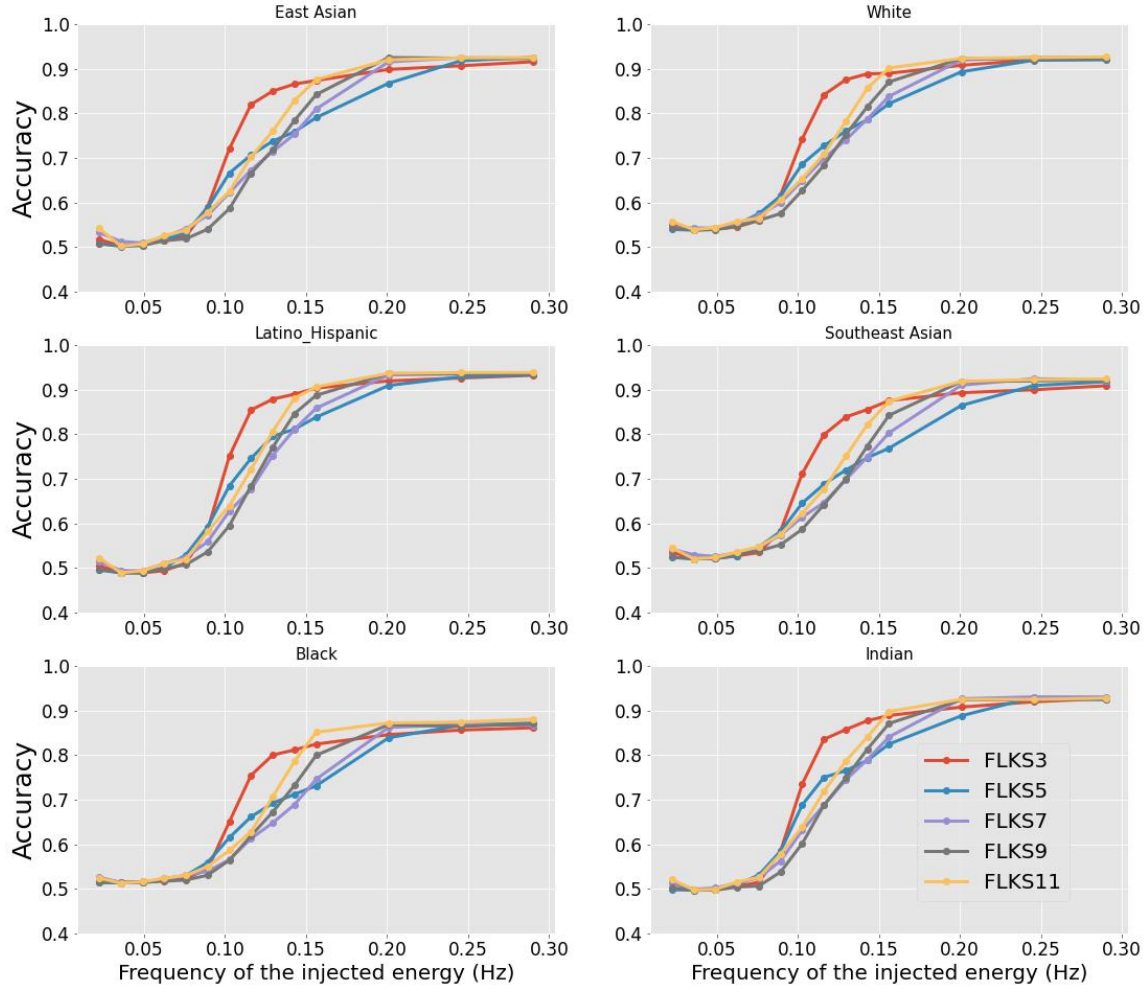


Fig. 8. **Frequency energy injection result.** We show models' performances with different FLKS for 6 race groups separately (We ignore Mid. Eastern since it has unequal number of samples for different genders in the test dataset). In each individual figure, the x-axis is the frequency we are injecting energy at and the y-axis is the accuracy of different models. It is obvious that all the models suffer from low to mid frequency's energy injections, and become robust to mid to high frequency noises. It is hard to directly tell which group is getting influenced more than the others, which furthers asks for a quantitatively analysis.

the Black group in frequency group 1 is also significantly smaller than those of the other groups. As the frequency increases, this gap reduces.

5 DISCUSSION AND CONCLUSION

Our results in Figs. 5, 6, 7, 8, 9 first demonstrate that smaller convolutional kernel sizes can cause a CNN to be biased towards high-frequency features, and increasing the kernel size mitigates this bias. We also see that such frequency bias significantly differed across different race/gender subgroups. All models trained on the two datasets focused less on high-frequency features for the Black and Male subgroup. While different features do not necessarily indicate

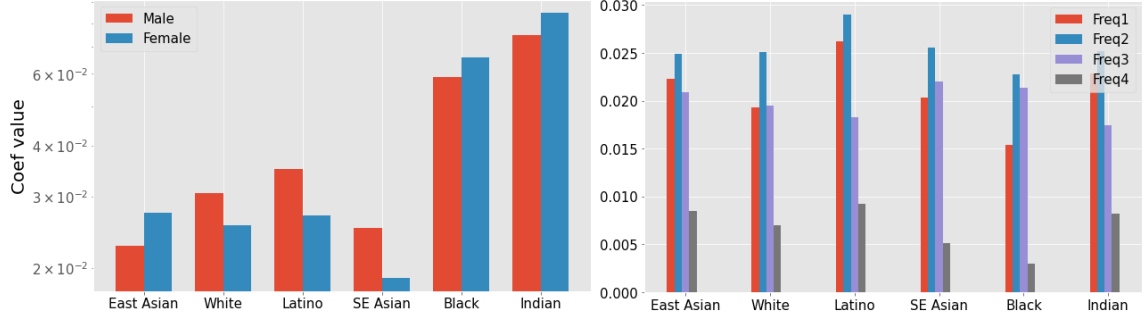


Fig. 9. **Regression coefficient values for β for different race groups.** (a) β values for the regression in Sec. 4.1.3 linking kernel size to adversarial perturbation distance, also shown in Table 2. There are significant differences across protected groups, e.g., the Black and Indian group has significant higher values compared to the other groups. (b) β values for the regression in Sec. 4.2.1. The coefficients for Black are always lower than those of other race groups. In addition, the coefficient values for different frequencies within the same race group are also significantly different.

performance bias on test samples, our results allow us to conclude that these differences do lead to performance biases on out-of-distribution (OOD) samples. We observed that this is the case for two different types of OOD image perturbation operators: adversarial attacks and frequency domain energy injections. As expected, kernel size has no effect on model performance on within-distribution test samples (Table 1).

Different population subgroups will have different image characteristics. For example, the Black group will likely have darker skin tones than other race groups, and Females will have more hair on average than Males. Hence, it is not surprising that there is some difference in how images from one race are processed by a network compared to another. However, our results indicate something more significant: that there is a fundamental difference in the frequency characteristics of the image features across groups used by the network to make its decision. This difference may also lead to a performance bias, depending on the type of OOD data model is faced with. Our two OOD perturbations, while conceptually clear and well-motivated, are not associated with any real phenomena. It would be an interesting next step to relate frequency biases of features to disparate model performance on real-world OOD artifacts like shot noise, fog, and motion blur [66].

Our work has several limitations. We cannot draw broad conclusions about the nature of kernel size for general CNNs across all applications, as we focused on a single application of interest (gender classification). Our aim in this work was to demonstrate that a hyperparameter may have a disparate impact on the internal biases of a network, and to that end our experiments succeeded. A further evaluation on a wider set of application domains is an important next step. We also limited our causal analyses to a few key variables. However, causal analysis typically relies on the “no hidden confounders” assumption. An exhaustive set of image factors will help in computing more precise causal effects.

We focused on convolutional kernel size of a network in this work due to past results establishing a clear link between this hyperparameter and frequency content [8]. However, our framework is agnostic to the nature of the hyperparameter. Indeed, next steps in this research space include similar analyses into a more comprehensive set of network hyperparameters, such as activation functions, depth of layers, weight initialization strategies, and even high-level designs (e.g., residual connections, transformer modules). We see our work as a first step in the important

direction of understanding how neural network design choices impact bias, and hence, the fairness of these systems in our society.

REFERENCES

- [1] Vitor Albiero, Krishnapriya Ks, Kushal Vangara, Kai Zhang, Michael C King, and Kevin W Bowyer. 2020. Analysis of gender inequality in face recognition accuracy. In *Proceedings of the IEEE/CVF winter conference on applications of computer vision workshops*. 81–89.
- [2] Guha Balakrishnan, Yuanjun Xiong, Wei Xia, and Pietro Perona. 2021. Towards causal benchmarking of biasin face analysis algorithms. In *Deep Learning-Based Face Analytics*. Springer, 327–359.
- [3] Alex Beutel, Jilin Chen, Tulsee Doshi, Hai Qian, Li Wei, Yi Wu, Lukasz Heldt, Zhe Zhao, Lichan Hong, Ed H. Chi, and Cristos Goodrow. 2019. Fairness in recommendation ranking through pairwise comparisons. In *ACM International Conference on Knowledge Discovery and Data Mining (KDD)*.
- [4] Alex Beutel, Jilin Chen, Zhe Zhao, and Ed Huai-hsin Chi. 2017. Data Decisions and Theoretical Implications when Adversarially Learning Fair Representations. *CoRR* abs/1707.00075 (2017).
- [5] Sébastien Bubeck, Eric Price, and Ilya Razenshteyn. 2018. Adversarial examples from computational constraints. *arXiv preprint arXiv:1805.10204* (2018).
- [6] Joy Buolamwini and Timnit Gebru. 2018. Gender shades: Intersectional accuracy disparities in commercial gender classification. In *Conference on Fairness, Accountability and Transparency*.
- [7] Nicholas Carlini and David Wagner. 2017. Towards evaluating the robustness of neural networks. In *2017 IEEE Symposium on Security and Privacy (SP)*. Ieee, 39–57.
- [8] Josue Ortega Caro, Yilong Ju, Ryan Pyle, Sourav Dey, Wieland Brendel, Fabio Anselmi, and Ankit Patel. 2020. Local convolutions cause an implicit bias towards high frequency adversarial examples. *arXiv preprint arXiv:2006.11440* (2020).
- [9] Kristy Choi, Aditya Grover, Trisha Singh, Rui Shu, and Stefano Ermon. 2020. Fair generative modeling via weak supervision. In *International Conference on Machine Learning (ICML)*.
- [10] Sam Corbett-Davies and Sharad Goel. 2018. The measure and mismeasure of fairness: A critical review of fair machine learning. *arXiv preprint arXiv:1808.00023* (2018).
- [11] Mengnan Du, Fan Yang, Na Zou, and Xia Hu. 2020. Fairness in deep learning: A computational perspective. *IEEE Intelligent Systems* 36, 4 (2020), 25–34.
- [12] Harrison Edwards and Amos J. Storkey. 2016. Censoring Representations with an Adversary. In *International Conference on Learning Representations (ICLR)*.
- [13] Fartash Faghri, Sven Gowal, Cristina Vasconcelos, David J Fleet, Fabian Pedregosa, and Nicolas Le Roux. 2021. Bridging the gap between adversarial robustness and optimization bias. *arXiv preprint arXiv:2102.08868* (2021).
- [14] Alhussein Fawzi, Hamza Fawzi, and Omar Fawzi. 2018. Adversarial vulnerability for any classifier. In *Advances in Neural Information Processing Systems*. 1178–1187.
- [15] Nic Ford, Justin Gilmer, Nicolas Carlini, and Dogus Cubuk. 2019. Adversarial examples are a natural consequence of test error in noise. *arXiv preprint arXiv:1901.10513* (2019).
- [16] Yaroslav Ganin and Victor Lempitsky. 2015. Unsupervised domain adaptation by backpropagation. In *International conference on machine learning*. PMLR, 1180–1189.
- [17] Justin Gilmer, Luke Metz, Fartash Faghri, Samuel S Schoenholz, Maithra Raghu, Martin Wattenberg, and Ian Goodfellow. 2018. Adversarial spheres. *arXiv preprint arXiv:1801.02774* (2018).
- [18] Ian J Goodfellow, Jonathon Shlens, and Christian Szegedy. 2014. Explaining and harnessing adversarial examples. *arXiv preprint arXiv:1412.6572* (2014).
- [19] Patrick Grother, Mei Ngan, and Kayee Hanaoka. 2019. *Face recognition vendor test (fvt): Part 3, demographic effects*. National Institute of Standards and Technology Gaithersburg, MD.
- [20] Aditya Grover, Jiaming Song, Alekh Agarwal, Kenneth Tran, Ashish Kapoor, Eric Horvitz, and Stefano Ermon. 2019. Bias correction of learned generative models using likelihood-free importance weighting. *arXiv preprint arXiv:1906.09531* (2019).
- [21] Moritz Hardt, Eric Price, and Nati Srebro. 2016. Equality of opportunity in supervised learning. *Advances in neural information processing systems* 29 (2016).
- [22] Kaiming He, Xiangyu Zhang, Shaoqing Ren, and Jian Sun. 2016. Deep residual learning for image recognition. In *Proceedings of the IEEE conference on computer vision and pattern recognition*. 770–778.
- [23] Lisa Anne Hendricks, Kaylee Burns, Kate Saenko, Trevor Darrell, and Anna Rohrbach. 2018. Women also snowboard: Overcoming bias in captioning models. In *Proceedings of the European Conference on Computer Vision (ECCV)*. 771–787.
- [24] Gao Huang, Zhuang Liu, Laurens Van Der Maaten, and Kilian Q Weinberger. 2017. Densely connected convolutional networks. In *Proceedings of the IEEE conference on computer vision and pattern recognition*. 4700–4708.
- [25] Andrew Ilyas, Shibani Santurkar, Dimitris Tsipras, Logan Engstrom, Brandon Tran, and Aleksander Madry. 2019. Adversarial examples are not bugs, they are features. In *Advances in Neural Information Processing Systems*. 125–136.
- [26] Michael Kane. 2010. Validity and fairness. *Language testing* 27, 2 (2010), 177–182.
- [27] Nikos Karantzas, Emma Besier, Josue Ortega Caro, Xaq Pitkow, Andreas S Tolias, Ankit B Patel, and Fabio Anselmi. 2022. Understanding robustness and generalization of artificial neural networks through Fourier masks. *Frontiers in Artificial Intelligence* 5 (2022).

- [28] Kimmo Kärkkäinen and Jungseock Joo. 2019. Fairface: Face attribute dataset for balanced race, gender, and age. *arXiv preprint arXiv:1908.04913* (2019).
- [29] Kimmo Karkkainen and Jungseock Joo. 2021. Fairface: Face attribute dataset for balanced race, gender, and age for bias measurement and mitigation. In *Proceedings of the IEEE/CVF Winter Conference on Applications of Computer Vision*. 1548–1558.
- [30] Michael Kearns, Seth Neel, Aaron Roth, and Zhiwei Steven Wu. 2018. Preventing fairness gerrymandering: Auditing and learning for subgroup fairness. In *International Conference on Machine Learning*. PMLR, 2564–2572.
- [31] Byungju Kim, Hyunwoo Kim, Kyungsu Kim, Sungjin Kim, and Junmo Kim. 2019. Learning not to learn: Training deep neural networks with biased data. In *IEEE Conference on Computer Vision and Pattern Recognition (CVPR)*.
- [32] Brendan F Klare, Mark J Burge, Joshua C Klontz, Richard W Vorder Bruegge, and Anil K Jain. 2012. Face recognition performance: Role of demographic information. *IEEE Transactions on Information Forensics and Security* 7, 6 (2012), 1789–1801.
- [33] Jon Kleinberg, Jens Ludwig, Sendhil Mullainathan, and Cass R Sunstein. 2018. Discrimination in the Age of Algorithms. *Journal of Legal Analysis* 10 (2018), 113–174.
- [34] Matthäus Kleindessner, Samira Samadi, Muhammad Bilal Zafar, Krishnamurthy Kethapadi, and Chris Russell. 2022. Pairwise Fairness for Ordinal Regression. (2022). *International Conference on Artificial Intelligence and Statistics (AISTATS)*.
- [35] Adam Kortylewski, Bernhard Egger, Andreas Schneider, Thomas Gerig, Andreas Morel-Forster, and Thomas Vetter. 2018. Empirically analyzing the effect of dataset biases on deep face recognition systems. In *Proceedings of the IEEE Conference on Computer Vision and Pattern Recognition Workshops*.
- [36] Adam Kortylewski, Bernhard Egger, Andreas Schneider, Thomas Gerig, Andreas Morel-Forster, and Thomas Vetter. 2019. Analyzing and reducing the damage of dataset bias to face recognition with synthetic data. In *Proceedings of the IEEE/CVF Conference on Computer Vision and Pattern Recognition Workshops*.
- [37] Chong M Lau, Kuan M Wong, and Ian RC Eggleton. 2008. Fairness of performance evaluation procedures and job satisfaction: The role of outcome-based and non-outcome-based effects. *Accounting and business research* 38, 2 (2008), 121–135.
- [38] Yi Li and Nuno Vasconcelos. 2019. Repair: Removing representation bias by dataset resampling. In *IEEE Conference on Computer Vision and Pattern Recognition (CVPR)*.
- [39] Zhe Li, Josue Ortega Caro, Evgenia Rusak, Wieland Brendel, Matthias Bethge, Fabio Anselmi, Ankit B Patel, Andreas S Tolias, and Xaq Pitkow. 2022. Robust deep learning object recognition models rely on low frequency information in natural images. *bioRxiv* (2022).
- [40] Michael Lohaus, Michael Perrot, and Ulrike von Luxburg. 2020. Too Relaxed to Be Fair. In *International Conference on Machine Learning (ICML)*.
- [41] David Madras, Elliot Creager, Toniann Pitassi, and Richard S. Zemel. 2018. Learning Adversarially Fair and Transferable Representations. In *International Conference on Machine Learning (ICML)*.
- [42] Saeed Mahloujifar, Dimitrios I Diochnos, and Mohammad Mahmoody. 2019. The curse of concentration in robust learning: Evasion and poisoning attacks from concentration of measure. In *Proceedings of the AAAI Conference on Artificial Intelligence*, Vol. 33. 4536–4543.
- [43] Michele Merler, Nalini Rath, Rogerio S Feris, and John R Smith. 2019. Diversity in faces. *arXiv preprint arXiv:1901.10436* (2019).
- [44] Alejandro Noriega-Campero, Michiel A Bakker, Bernardo Garcia-Bulle, and Alex'Sandy' Pentland. 2019. Active fairness in algorithmic decision making. In *Proceedings of the 2019 AAAI/ACM Conference on AI, Ethics, and Society*. 77–83.
- [45] Manisha Padala and Sujit Gujar. 2020. FNFC: Achieving Fairness through Neural Networks. In *International Joint Conferences on Artificial Intelligence Organization (IJCAI)*.
- [46] Jean Ponce, Tamara L Berg, Mark Everingham, David A Forsyth, Martial Hebert, Svetlana Lazebnik, Marcin Marszalek, Cordelia Schmid, Bryan C Russell, Antonio Torralba, et al. 2006. Dataset issues in object recognition. In *Toward category-level object recognition*. Springer, 29–48.
- [47] Novi Quadrianto, Viktoriia Sharmanska, and Oliver Thomas. 2019. Discovering fair representations in the data domain. In *Proceedings of the IEEE/CVF conference on computer vision and pattern recognition*. 8227–8236.
- [48] Vikram V Ramaswamy, Sunnie SY Kim, and Olga Russakovsky. 2021. Fair attribute classification through latent space de-biasing. In *Proceedings of the IEEE/CVF conference on computer vision and pattern recognition*. 9301–9310.
- [49] Vikram V. Ramaswamy, Sunnie S. Y. Kim, and Olga Russakovsky. 2021. Fair Attribute Classification through Latent Space De-biasing. In *IEEE Conference on Computer Vision and Pattern Recognition (CVPR)*.
- [50] Laurent Risser, Quentin Vincenot, and Jean-Michel Loubes. 2020. Tackling Algorithmic Bias in Neural-Network Classifiers using Wasserstein-2 Regularization. *arXiv:1908.05783* [stat.ML]
- [51] Prasanna Sattigeri, Samuel C Hoffman, Vijil Chenthamarakshan, and Kush R Varshney. 2019. Fairness GAN: Generating datasets with fairness properties using a generative adversarial network. *IBM Journal of Research and Development* 63, 4/5 (2019), 3–1.
- [52] Ludwig Schmidt, Shibani Santurkar, Dimitris Tsipras, Kunal Talwar, and Aleksander Madry. 2018. Adversarially robust generalization requires more data. In *Advances in Neural Information Processing Systems*. 5014–5026.
- [53] Karen Simonyan and Andrew Zisserman. 2014. Very deep convolutional networks for large-scale image recognition. *arXiv preprint arXiv:1409.1556* (2014).
- [54] Chandan Singh, Guha Balakrishnan, and Pietro Perona. 2021. Matched sample selection with GANs for mitigating attribute confounding. *arXiv preprint arXiv:2103.13455* (2021).
- [55] Megha Srivastava, Hoda Heidari, and Andreas Krause. 2019. Mathematical notions vs. human perception of fairness: A descriptive approach to fairness for machine learning. In *Proceedings of the 25th ACM SIGKDD international conference on knowledge discovery & data mining*. 2459–2468.

- [56] Thomas Tanay and Lewis Griffin. 2016. A boundary tilting perspective on the phenomenon of adversarial examples. *arXiv preprint arXiv:1608.07690* (2016).
- [57] Antonio Torralba and Alexei A Efros. 2011. Unbiased look at dataset bias. In *CVPR 2011*. IEEE, 1521–1528.
- [58] Sriram Vasudevan and Krishnamurthy Kenthapadi. 2020. Lift: A scalable framework for measuring fairness in ml applications. In *Proceedings of the 29th ACM International Conference on Information & Knowledge Management*. 2773–2780.
- [59] Haohan Wang, Xindi Wu, Zeyi Huang, and Eric P Xing. 2020. High-frequency Component Helps Explain the Generalization of Convolutional Neural Networks. In *Proceedings of the IEEE/CVF Conference on Computer Vision and Pattern Recognition*. 8684–8694.
- [60] Mei Wang, Weihong Deng, Jiani Hu, Xunqiang Tao, and Yaohai Huang. 2019. Racial faces in the wild: Reducing racial bias by information maximization adaptation network. In *Proceedings of the IEEE/CVF international conference on computer vision*. 692–702.
- [61] Tianlu Wang, Jieyu Zhao, Mark Yatskar, Kai-Wei Chang, and Vicente Ordonez. 2019. Balanced datasets are not enough: Estimating and mitigating gender bias in deep image representations. In *Proceedings of the IEEE/CVF International Conference on Computer Vision*. 5310–5319.
- [62] Zeyu Wang, Klint Qinami, Ioannis Karakozis, Kyle Genova, Prem Nair, Kenji Hata, and Olga Russakovsky. 2020. Towards Fairness in Visual Recognition: Effective Strategies for Bias Mitigation. In *IEEE Conference on Computer Vision and Pattern Recognition (CVPR)*.
- [63] Zeyu Wang, Klint Qinami, Ioannis Christos Karakozis, Kyle Genova, Prem Nair, Kenji Hata, and Olga Russakovsky. 2020. Towards fairness in visual recognition: Effective strategies for bias mitigation. In *Proceedings of the IEEE/CVF conference on computer vision and pattern recognition*. 8919–8928.
- [64] Michael Wick, Swetasudha Panda, and Jean-Baptiste Tristan. 2019. Unlocking Fairness: a Trade-off Revisited. In *Neural Information Processing Systems (NeurIPS)*.
- [65] Jeffrey M Wooldridge. 2010. *Econometric analysis of cross section and panel data*. MIT press.
- [66] Dong Yin, Raphael Gontijo Lopes, Jonathon Shlens, Ekin D. Cubuk, and Justin Gilmer. 2019. *A Fourier Perspective on Model Robustness in Computer Vision*. Curran Associates Inc., Red Hook, NY, USA.
- [67] Rich Zemel, Yu Wu, Kevin Swersky, Toni Pitassi, and Cynthia Dwork. 2013. Learning fair representations. In *International conference on machine learning*. PMLR, 325–333.
- [68] Rich Zemel, Yu Wu, Kevin Swersky, Toni Pitassi, and Cynthia Dwork. 2013. Learning fair representations. In *International Conference on Machine Learning (ICML)*.
- [69] Brian Hu Zhang, Blake Lemoine, and Margaret Mitchell. 2018. Mitigating unwanted biases with adversarial learning. In *Proceedings of the 2018 AAAI/ACM Conference on AI, Ethics, and Society*. 335–340.
- [70] Song Yang Zhang, Zhifei and Hairong Qi. 2017. Age Progression/Regression by Conditional Adversarial Autoencoder. In *IEEE Conference on Computer Vision and Pattern Recognition (CVPR)*. IEEE.
- [71] Dominik Zietlow, Michael Lohaus, Guha Balakrishnan, Matthäus Kleindessner, Francesco Locatello, Bernhard Schölkopf, and Chris Russell. 2022. Leveling Down in Computer Vision: Pareto Inefficiencies in Fair Deep Classifiers. In *Proceedings of the IEEE/CVF Conference on Computer Vision and Pattern Recognition*. 10410–10421.
- [72] James Zou and Londa Schiebinger. 2018. AI can be sexist and racist—it’s time to make it fair.

Supplemental Materials

A EXPERIMENT SETUP

A.1 Training details

The models were trained in a multi-task style. During training, the model was required to predict labels of race&gender&gender of a training sample, while during inference we only use the gender label predicted by the model. For training hyperparameters, we used a batch-size of 128, an initial learning rate of $1e^{-3}$ which decays by 10 times at epoch 13 and epoch 17. We trained all the models with a total number of 21 epochs. We used an Adam optimizer.

A.2 Computing resources

All the experiments were run with NVIDIA Tesla A100 GPUs. Training a model per run took 1 GPU hour. Applying FGSM attack to test dataset of FairFace took $\sim 1,000$ seconds, applying CW attack to test dataset of FairFace took $\sim 6,000$ seconds.

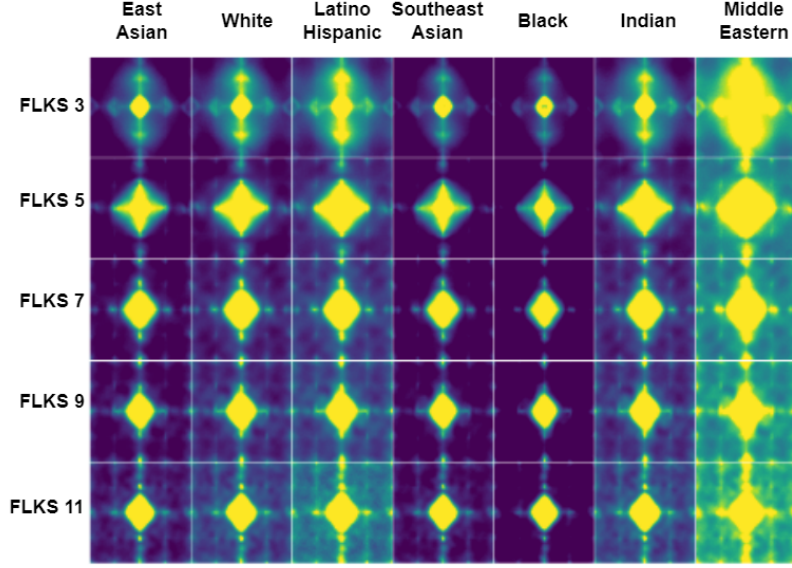


Fig. 10. **Perturbation Spectrum Visualization on Fairface using DenseNet121.** Similar to results in Fig. 5 and 6, each row represents a model with a different First Layer Kernel Size (FLKS), and each column corresponds to protected attribute groups. We observed a similar trending as discovered in the other 2 results above: generally, the perturbation shifts its attention to low-frequency information as FLKS increases, and the perturbations for Black always have lower high-frequency focus compared to other race group.

B RESULTS ON DENSENET121

To further test the robustness and universality of our framework and conclusion, we also tested on DenseNet121 – another popular face analysis model. We also vary the first convolutional kernel size from $\{3, 5, 7, 9, 11\}$. We report the averaged spectra in Fig. 10, and its corresponding perturbation distance & $f_{0.5}$ scores in Fig. 11.

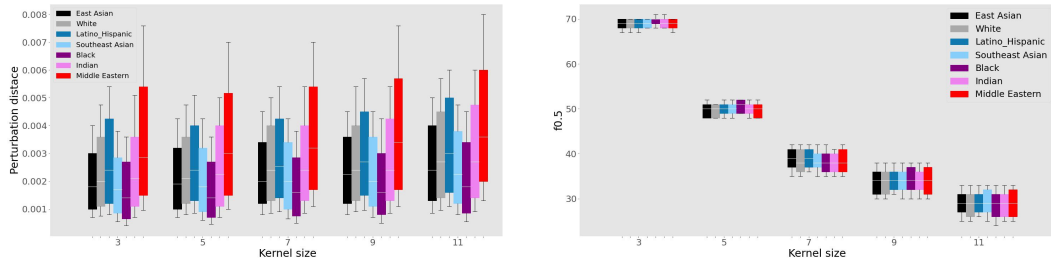


Fig. 11. **Perturbation spectra $f_{0.5}$ & Perturbation distance for DenseNet121.** We visualize the perturbation and $f_{0.5}$ scores in the same way discussed in Sec. 4.1.1, 4.1.2 and Fig. 7. We observed a similar trend: there is a significant trend that the $f_{0.5}$ drops as the FLKS increases for all demographic groups and as the FLKS increases, the perturbation distances generally increase too for all the demographic groups.

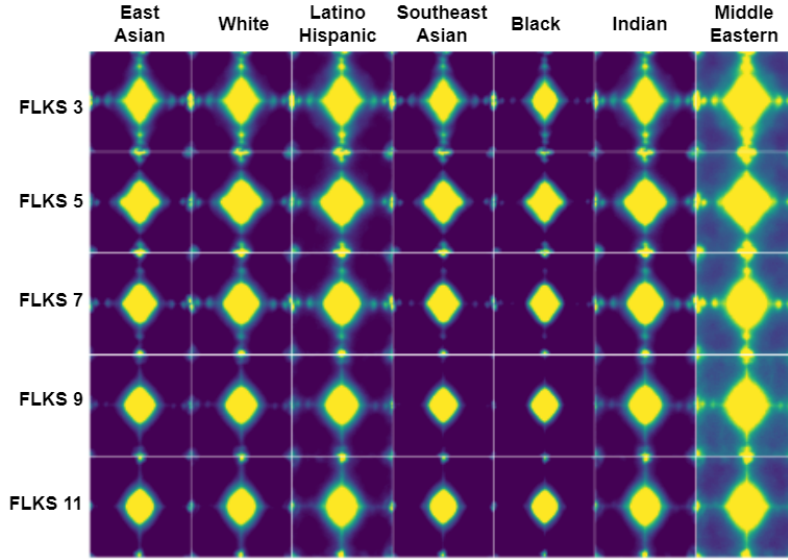


Fig. 12. **Perturbation Spectrum Visualization on Fairface using Vgg16.** Similar to results in Fig. 5 and 6, each row represents a model with a different First Layer Kernel Size (FLKS), and each column corresponds to protected attribute groups. We observed a similar trending as discovered in the other 2 results above: generally, the perturbation shifts its attention to low-frequency information as FLKS increases, and the perturbations for Black always have lower high-frequency focus compared to other race group.

C RESULTS ON VGG16

To further test the robustness and universality of our framework and conclusion, we also tested on Vgg16— another popular face analysis model. We also vary the first convolutional kernel size from $\{3, 5, 7, 9, 11\}$. We report the averaged spectra in Fig. 12, and its corresponding perturbation distance & $f_{0.5}$ scores in Fig. 13.

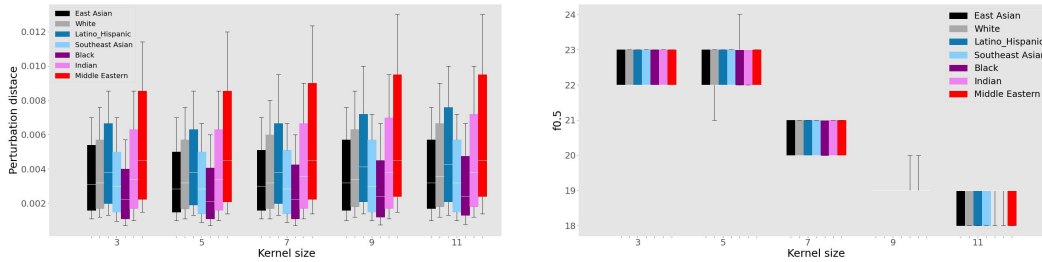


Fig. 13. **Perturbation spectra $f_{0.5}$ & Perturbation distance for Vgg16.** We visualize the perturbation and $f_{0.5}$ scores in the same way discussed in Sec. 4.1.1, 4.1.2 and Fig. 7. We observed a similar trend: there is a significant trend that the $f_{0.5}$ drops as the FLKS increases for all demographic groups and as the FLKS increases, the perturbation distances generally increase too for all the demographic groups.

D RESULTS OF VARYING ALL CONVOLUTIONAL KERNEL SIZES

We also test our framework on the occasion where we modify all the convolutional layers' kernel sizes. The results are in Fig. 14. Basically, we found that modifying all convolutional layers' kernel sizes doesn't make a significant difference comparing to *only* modify the first convolutional kernel size. Refer to the caption for more details.

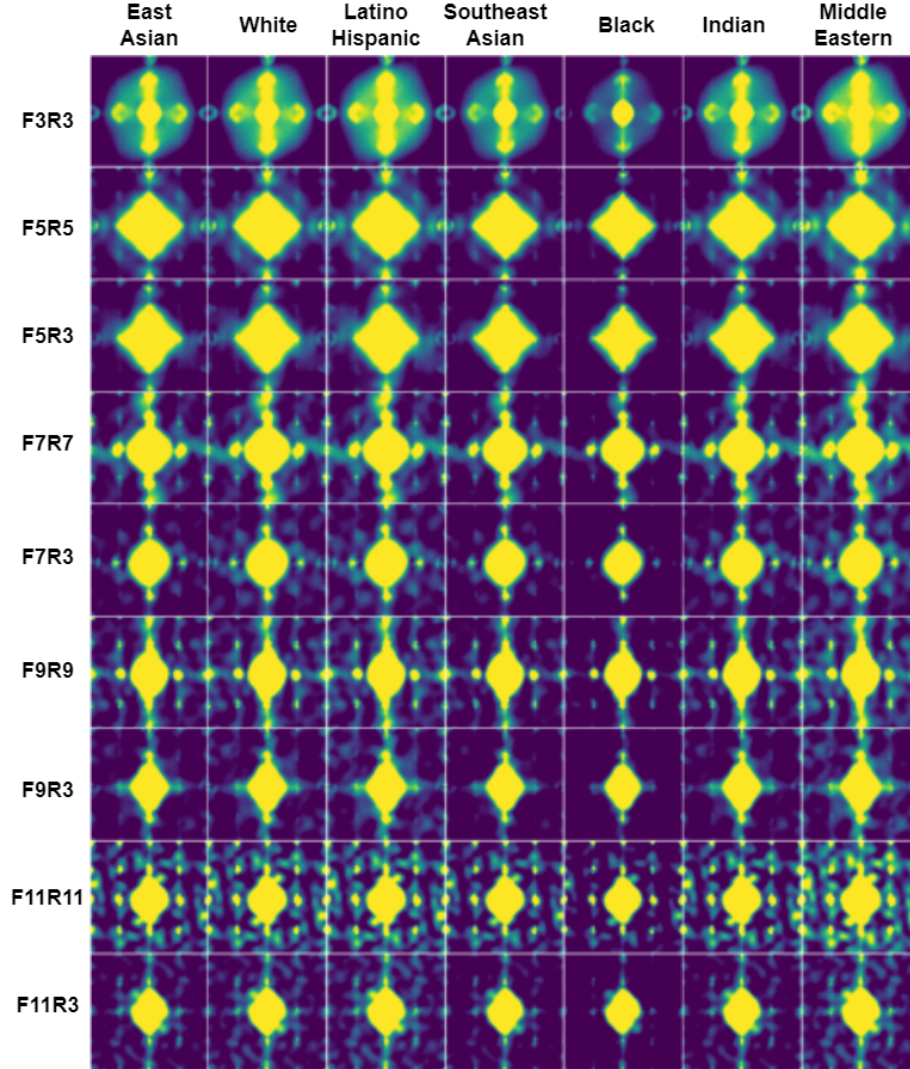


Fig. 14. **Perturbation Spectrum Visualization on Fairface for modifying all convolutional layer kernel size.** Each row represents a model with a different architectural choice, for example, “F3R3” represents model with first layer kernel size of 3 and the rest layers kernel sizes of 3, and each column corresponds to protected attribute groups. We found that modifying all convolutional layers' kernel sizes doesn't make a significant difference comparing to *only* modify the first convolutional kernel size.

E RESULTS OF APPLYING FGSM TO MODEL

We also test our framework on the occasion where we apply FGSM attack to all the models trained on Fairface. The results are in Fig. 15. It has basically the same trend with all the pervious spetra visualization.

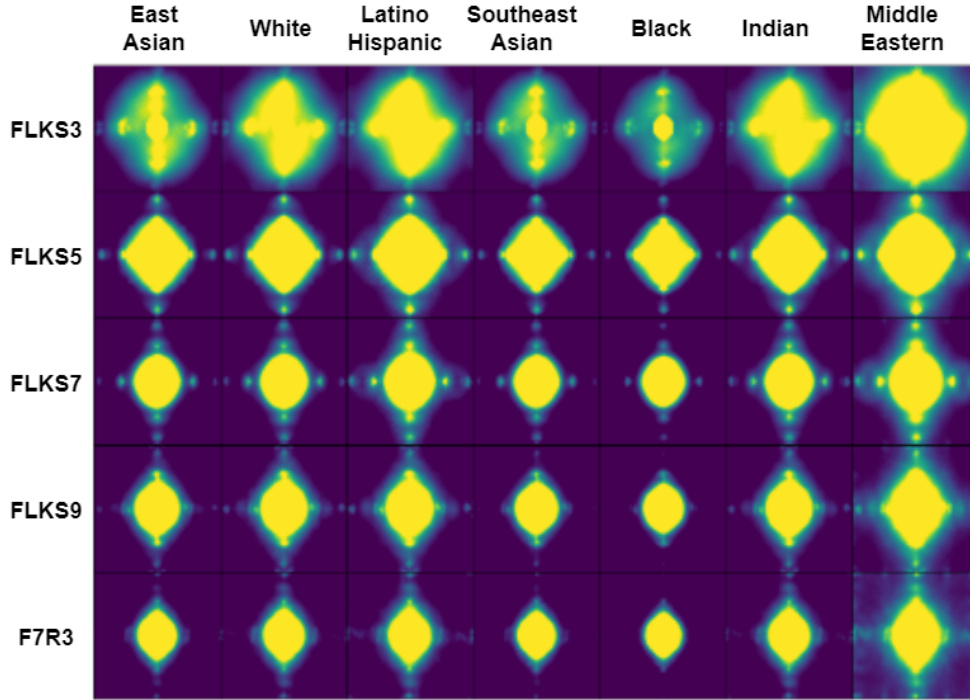


Fig. 15. **Perturbation Spectrum Visualization on Fairface using FGSM.** Similar to results in Fig. 5, each row represents a model with a different First Layer Kernel Size (FLKS), and each column corresponds to protected attribute groups. We observed a similar trending: generally, the perturbation shifts its attention to low-frequency information as FLKS increases, and the perturbations for Black always have lower high-frequency focus compared to other race group.